

The dynamics of a highly magnetized jet propagating inside a star

Omer Bromberg^{1,4}, Jonathan Granot², Yuri Lyubarsky³, Tsvi Piran⁴

¹Department of Astrophysical Sciences, Princeton University, 4 Ivy Ln., Princeton NJ 08544, USA

²Department of Natural Sciences, The Open University of Israel, P.O.B 808, Ra'anana 43537, Israel

³Physics Department, Ben-Gurion University, P.O.B. 653, Beer-Sheva 84105, Israel

⁴Racah Institute of Physics, The Hebrew University, Jerusalem 91904, Israel

Abstract

The collapsar model explains the association of long duration gamma-Ray Bursts (GRBs) with stellar collapse. It involves a relativistic jet that forms at the core of a collapsing massive star. The jet penetrates the stellar envelope and the prompt GRB emission is produced once the jet is well outside the star. Most current models for generation of relativistic jets involve Poynting flux dominated outflows. We explore here the propagation of such a jet through a stellar envelope. The jet forms a bow shock around it. Energy dissipation at the head of this shock supplies energy to a cocoon that surrounds the jet. This cocoon exerts pressure on the jet and collimates it. While this description resembles the propagation of a hydrodynamic jets there are significant qualitative differences. Two Strong shocks, the reverse shock that slows down the hydrodynamic jet and the collimation shock that collimates it, cannot form within the Poynting flux dominated jet. As a result this jet moves much faster and dissipates much less energy while it crosses the stellar envelope. We construct here a simple analytic model that explores, self consistently, the jet-cocoon interaction and dynamics. Using this model we determine the properties of the jet, including its velocity, propagation time and shape.

1 introduction

Gamma-ray bursts (GRBs) are short and intense bursts of low energy gamma rays. They involve powerful relativistic jets. Long GRBs are associated with death of massive stars. The collapsar model¹ (Woosley, 1993; MacFadyen & Woosley, 1999) combined these two facts. According to this model a compact object is formed at the center of a star following its core collapse. This compact object launches a jet that drills a hole through the star and

¹Note that we use here a general definition of the collapsar model in which it involves any central engine that launches a jet within a collapsing star. This is regardless of the specific nature of the central engine.

breaks out through the surface. The observed gamma-rays are emitted due to some internal dissipation process far from the surface of the star. Clearly the propagation phase of the jet within the star is an essential ingredient of the model and in recent years a lot of numerical (e.g. MacFadyen, Woosley & Heger, 2001; Zhang, Woosley & MacFadyen, 2003; Morsony, Lazzati & Begelman, 2007; Mizuta & Aloy, 2009; Mizuta & Ioka, 2013) and analytic (e.g. Matzner, 2003; Lazzati & Begelman, 2005; Morsony, Lazzati & Begelman, 2007; Bromberg et al., 2011) efforts was devoted to explore the propagation of a hydrodynamics jets within stars.

Most current relativistic jet models are based in one way or another on a central engine that generate a collimated Poynting flux dominated outflow. This is partially motivated due to analogy with AGNs. For AGNs, Poynting flux is the only available option. In GRBs a thermally driven jet (a fireball) is also thermodynamically possible. Still it is generally expected that those will be less powerful than the electromagnetic ones (see e.g. Kawanaka, Piran & Krolik, 2013). It is therefore important to investigate the properties of a magnetic jet that propagates in the star, and whether its typical properties agrees with the observational constraints.

Collimated relativistic MHD jets in stellar environments were studied extensively both numerically and analytically under the approximation of an axi-symmetric, steady, non-dissipative flow (e.g. Komissarov et al., 2007, 2009; Tchekhovskoy, McKinney & Narayan, 2008b,a, 2009; Zakamska, Begelman & Blandford, 2008; Lyubarsky, 2009, 2010, 2011; Tchekhovskoy, Narayan & McKinney, 2010; Kohler & Begelman, 2012). In these studies, however, either the shape of the jet or the profile of the confining medium was predetermined. In a case of a predetermined pressure Lyubarsky (2009, 2010, 2011) have shown analytically how the properties of the jet are determined by a given distribution of the confining pressure, assuming a steady state.

In realistic outflows, however, the confining pressure is built during the course of the jet propagation, and its profile depends on the details of this propagation. Therefore the properties of the propagating jet and the confining pressure should be determined self consistently. Recently, Levinson & Begelman (2013) conducted an analytic, self consistent analysis for the propagation of a magnetic jet in a medium. Their model involves some constraining assumptions on the cocoon that result in a cylindrical jet, having a cross section radius of the order of the light cylinder radius of the central object. In additions they assume that kink instability grows in the jet on a time scale which is comparable to a few light crossing time of the jet width. This have lead them to conclude that the magnetic the jet will be disrupted by kink instability deep in the star, and transform to a hydrodynamic jet. However, as we show here, the jet is expected to be much wider and it is most likely that the kink instability has no time to develop in the jet before it breaks out of the star. Therefore, we assume here that the jet remains axi-symmetric.

We study, the dynamics of a Poynting dominated jet that propagates inside the star. The dissipation of energy at the jet's head leads to the formation of a hot cocoon that surround the jet. The cocoon applies pressure on the jet and collimates it. We build a

self consistent analytic model that follows the time evolution of the jet and the cocoon. We show that the pressure in the cocoon is typically large enough to collimate the jet close to the source, so that different parts of the jet maintain strong causal connection with the jet’s axis. In this case the poloidal magnetic field is comparable to the toroidal field in the proper frame of the jet. This leads to a smooth transition of the jet material from a free expansion state, near the engine, to a collated state. We also show that the typical width of the propagating jet is of the order of a few 10s light cylinder radii, which imply that the main body of the jet is stable to kink modes and that the jet is likely to survive crossing the star. We compare our results with recent numerical simulations of a highly magnetized jet (Bromberg & Tchekhovskoy, 2014) and show that there is a good agreement between the numerical and the analytic results. Finally, we discuss the differences between the propagation of a magnetic jet and a hydrodynamic jet, focusing on the breakout time of the jet from the star. We show that the propagation velocity of magnetic jets is relativistic in most parts of the star (unlike hydrodynamic jets which propagate typically at sub relativistic velocities).

The paper is structured as follow: In section 2 we describe the overall picture and lay down our basic assumptions. We calculate, In section 3, the propagation velocity of the jet and show that it depends only on the properties of the confining medium near the jet’s head. We then proceed to describe the geometry of the jet and it’s cocoon (section 4), followed by a discussion on the conditions at the base of the jet and the collimation of the jet (section 5). In section 6 we discuss the stability of the jet and its survival inside the star. Finally, in section 7 we obtain engine minimal activity time for a jet breakout. This quantity is of outmost importance as it might be related to the observed plateau in the long GRB duration distribution (Bromberg et al., 2012).

2 The overall picture and the model assumptions

We work within the scope of the standard collapsar picture of GRBs, a central engine (accreting black hole, or a millisecond magnetar) is producing a jet that pushes its way through the progenitor star. We assume that the jet is dominated by Poynting flux. The properties of the jet are determined by the total luminosity, L_j , by the light cylinder radius, defined as $r_L = c/\Omega_0$, where Ω_0 is the angular velocity of the field lines, and by the initial magnetization (Michel magnetization; Michel, 1969), σ_0 , defined as the ratio of the Poynting flux and the rest mass flux. The magnetization, σ_0 is in fact the maximal Lorentz factor achievable by the jet. Observations place a lower limit of $\Gamma_{max} \gtrsim 100$ (e.g. Piran, 1995; Lithwick & Sari, 2001; Granot, Cohen-Tanugi & do Couto e Silva, 2008), implying $\sigma_0 \gtrsim 100$.

When the jet propagates in the stellar envelope a bow shock forms ahead of it. This shock heats the ambient medium forming a pressurized cocoon around the jet. The cocoon applies pressure on the jet and collimates it. Describing the properties of such system is

an involved problem, since the cocoon is produced by the jet while the jet's properties are determined by the pressure distribution in the cocoon. Therefore the properties of the jet and the cocoon must be found self consistently.

The overall morphology of the jet-cocoon system is sketched in Figure 1. We use cylindrical coordinates (z, r) , where the jet points along the z axis, and the central source is at the origin. The jet's head is located at $z = z_h$. Coordinates along the jet axis are characterized either by the distance from the source, z , or by the distance from the head, $\bar{z} = z_h - z$. The jet's width is denoted by $r_j(z)$ and the cocoon's width by $r_c(z)$. The jet's material generally moves relativistically with a Lorentz factor Γ_j . Therefore one can conveniently describe the flow in two frames: the lab frame and the local comoving frame. Quantities measured in the local comoving frame are denoted by $'$. When we discuss the properties of the jet's head and the cocoon region near the head, we use a third reference frame, the rest frame of the head. We mark it by $''$ to distinguish it from the comoving frame of the jet material.

Our model contains four regions: the jet, the jet's head (shown in a zoom in on the left side of Fig. 1), the cocoon and the external medium. Parameters relating to each of these regions are marked with the indices j - for the jet, h - for the head, c - for the cocoon, and 'ext' - for the external medium. The subscript L denotes parameters on the jet's light cylinder.

When the plasma is injected at the base of the jet, its internal pressure, p_j , is so large that initially it expands freely until the collimation point where the jet's pressure equals the cocoon's pressure, $p_j = p_c$. Above this point the jet is collimated by the cocoon's pressure. The transition to a collimated state is accompanied by oscillations in the jet's radius around the equilibrium state (Lyubarsky, 2009). These oscillations gradually decay in an expanding jet. We ignore these oscillations here and discuss only the average structure. The properties of the jet that is collimated by a given external pressure can be described as follows.

In a Poynting dominated jet the magnetic field beyond the light cylinder is dominated by the toroidal component. However when calculating the response of the jet to the pressure excreted by the cocoon we must include the pressure contribution from the poloidal components as well. The reason for that is that in a magnetic field that is predominantly azimuthal (toroidal), the hoop stress is nearly counterbalanced by the electric force (see e.g. Lyubarsky, 2009, 2011). The outflow is governed by the residual small stress $B_\phi^2 - E^2 \approx B_\phi'^2 \sim (B_\phi/\Gamma_j)^2$, therefore generally the pressure of the poloidal field cannot be neglected.

The overall structure and the dynamics of the flow depend crucially on how well different parts of the jet can communicate with each other across the flow (Zakamska, Begelman & Blandford, 2008; Komissarov et al., 2009; Lyubarsky, 2009, 2011; Tchekhovskoy, McKinney & Narayan, 2009; Tchekhovskoy, Narayan & McKinney, 2010; Granot, Komissarov & Spitkovsky, 2011). In our case the jet is so narrow that it remains strongly causally connected. This means that the flow can communicate with the boundary in a time that

is shorter than the time it takes it to double its radius. This implies the condition

$$u_j \theta_j < 1, \quad (1)$$

where $u_j \equiv \Gamma_j \beta_j$ is the spatial component of the four velocity and θ_j is the opening angle of the flow. In this regime, the jet maintains transverse magnetic equilibrium at any distance from the source. Here the difference between the magnetic hoop stress and the electric force is counterbalanced by the pressure of the poloidal field so that $B'_\phi \approx B'_p$. Taking into account that $B_\phi \propto 1/r$ and $B_p \propto 1/r^2$, this condition immediately implies that the Lorenz factor of the jet is proportional to the jet's cylindrical radius, $\Gamma_j \approx r_j/r_L$. In appendix A we show that this scaling could be generalized to the non-relativistic case so that generally

$$u_j \approx r_j/r_L. \quad (2)$$

Using this and $\theta_j \approx r_j/z$, the condition of the strong connection, Eq. (1) reduces to $r_j < \sqrt{r_L z}$ which is always fulfilled for our jet. The radius of the jet in the region where it is relativistic is found from the simple relation (Tchekhovskoy, McKinney & Narayan, 2008a; Komissarov et al., 2009; Lyubarsky, 2009, 2011)

$$r_j = r_L \left(\frac{p_L}{p_c} \right)^{1/4}, \quad (3)$$

where p_L is the jet's magnetic pressure at r_L .

3 The propagation velocity (The velocity of the jet's head)

When the magnetic fields components are in equilibrium they are comparable in the co-moving frame. In this case the proper velocity of the jet's material scales linearly with the jet's cylindrical radius (see Eq. 2). Note that u_j is primarily directed along the poloidal magnetic field lines, which inside the collimated jet can be approximated as the z direction. As the fast moving material in the jet approaches the jet's head it must slow down in order to match its velocity to that of the shocked ambient matter. Since shocks are weak and ineffective in highly magnetized flows, the matter decelerates gradually as it approaches the jet's head, where the jet becomes narrower. This is in contrast with the case of a hydrodynamic jet where there is a strong reverse shock, across which there is a strong and instantaneous deceleration (e.g. Bromberg et al., 2011).

We define the head of the jet as the region where α''_c , the angle between the normal to the bow shock and the z -axis in the rest frame of the head, is smaller than 1 (see Fig. 1). In the head, the magnetic pressure is balanced by the ram pressure of the ambient medium. We can express this pressure balance as:

$$\rho_{\text{ext}} c^2 u_h^2 \cos^2 \alpha''_c \approx p_j, \quad (4)$$

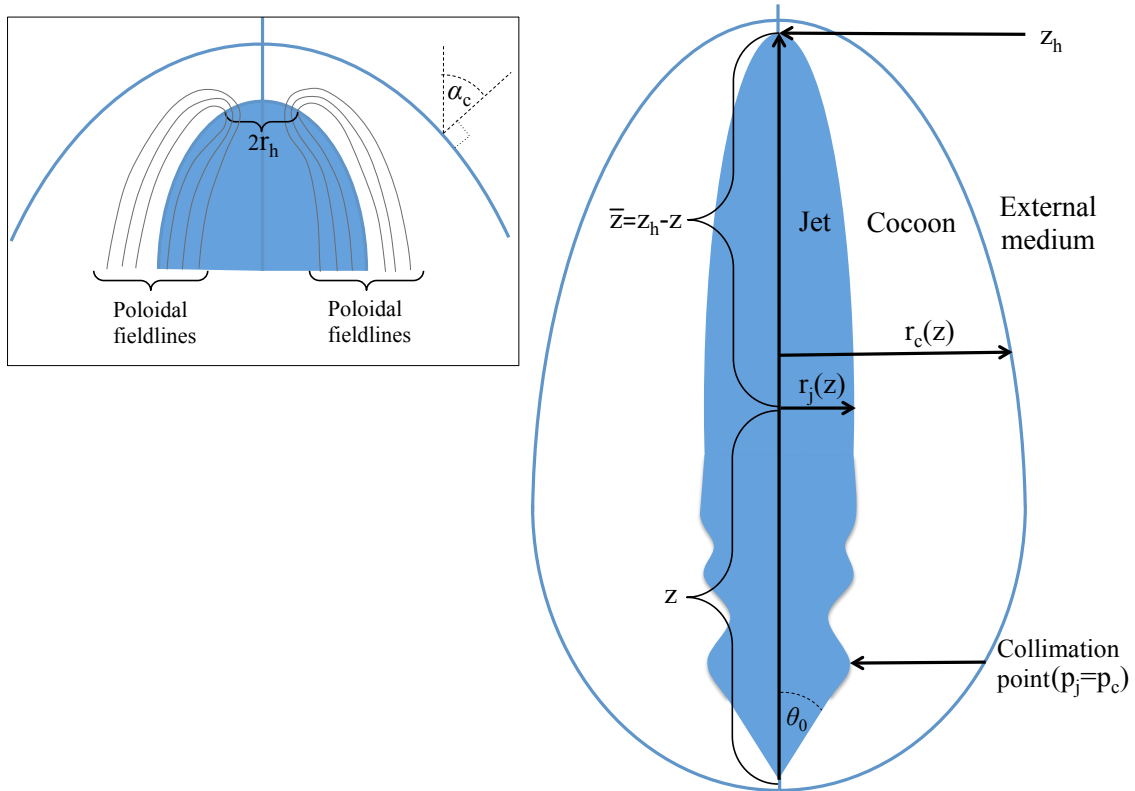


Figure 1: The morphology of the magnetic jet and its cocoon. The entire jet is shown on the right side and a zoom in on the head region is shown on the left. The jet (blue) is surrounded by a hot cocoon that applies pressure on it. The cocoon is bounded by a shock surface, that separates it from the external medium (solid blue line). Below the collimation point the jet's pressure (p_j) is larger than the pressure of the cocoon (p_c) and the jet expands along conical field lines. When $p_j = p_c$, the jet becomes collimated by the cocoon, and from there on it maintains pressure balance with it. The collimation is accompanied by oscillations in the jet's radius. As the jet expands these oscillations gradually die out. Close to the head p_c increases and as a result the jet's cross section decreases. The jet material decelerates until it's velocity matches the velocity of the shocked material ahead of the jet at a radius $r_j \simeq r_h$. The dashed horizontal line separates the relativistic part of the cocoon from the non-relativistic part. The former exists only when the jet's head moves at relativistic velocities.

where u_h is the proper velocity of the head and ρ_{ext} is the mass density of the ambient medium. Since the jet is highly magnetized its internal pressure can be approximated as $p_j = B'^2/8\pi \sim B_\phi'^2/4\pi = (B_\phi/\Gamma_j)^2/4\pi$. Taking the jet's dimensionless 3-velocity, β_j , the electric field is $E \simeq \beta_j B_\phi$, and the Poynting flux is

$$S = (c/4\pi)\beta_j B_\phi^2. \quad (5)$$

The electromagnetic luminosity of the jet is given by

$$L_j = \int 2\pi r dr S \approx (c/4)B_\phi^2 r_j^2 \beta_j \approx \pi r_j^2 \Gamma_j^2 \beta_j p_j c. \quad (6)$$

Substituting in Eqs. (2, 4) we obtain

$$\rho_{\text{ext}} c^2 u_h^2 \cos^2 \alpha_c'' \sim \frac{L_j}{\pi c r_L^2 \Gamma_j u_j^3}. \quad (7)$$

Near the head, $\cos \alpha_c'' \sim 1$ (the forward shock is roughly perpendicular to the z -axis). Substituting $u_j \sim u_h$, we get

$$\Gamma_h u_h^5 = (1 + u_h^2)^{1/2} u_h^5 \sim \frac{L_j}{\pi \rho_{\text{ext}} c^3 r_L^2}. \quad (8)$$

We define the dimensionless quantity

$$a \equiv \frac{L_j}{\pi \rho_{\text{ext}} c^3 r_L^2} = \frac{p_L}{\rho_{\text{ext}} c^2} \approx 1.2 \frac{L_{50}}{\rho_4 r_{L7}^2}, \quad (9)$$

which represents the ratio between the jet's magnetic pressure at the light cylinder and the ambient medium's rest mass energy density near the head. We use here and elsewhere the notation $q_x \equiv q/10^x$ in c.g.s. units. Now, Eqs. (8, 9) yield:

$$u_h \sim \frac{r_h}{r_L} \sim \begin{cases} a^{1/5} & (u_h \ll 1) , \\ a^{1/6} & (u_h \gg 1) . \end{cases} \quad (10)$$

Note that for a given jet (i.e. for a particular $p_L \propto L_j/r_L^2$) the parameter a , which determines the velocity and the cross-section of the jet's head, depends only on the ambient density near the head. Thus, Eq. (10) implies that the jet's propagation velocity is determined locally and it is insensitive to the geometry of the jet below the head.

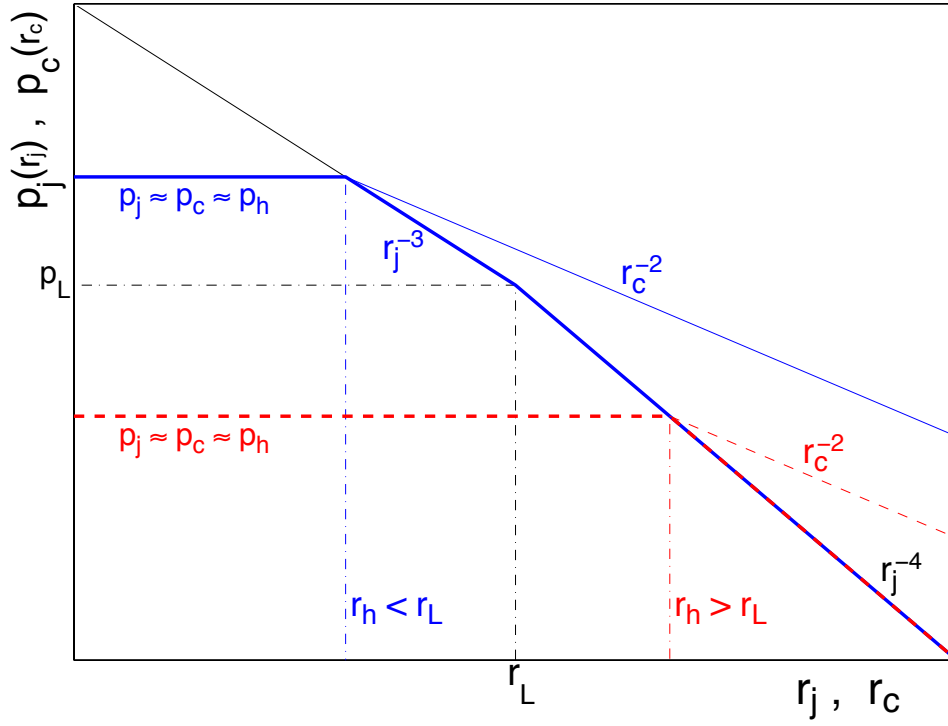


Figure 2: The pressure distribution across the jet, $p_j(r_j)$ (Thick line), and the cocoon, $p_c(r_c)$ (thin line). Solid line shows the distribution in a case of a non-relativistic head, and dashed lines for relativistic head.

4 The geometry of the cocoon

The energy in the cocoon originates from the work the jet preforms on the ambient medium. In the lab frame the differential work is $dE = p_j dV = p_j dA_\perp dz$, so that the power exerted by the jet is given by $\dot{E} = dE/dt = \int dA_\perp v_h p_j$, where $v_h = dz/dt$, $A_\perp = \vec{A} \cdot \hat{z}$, and $dA_\perp = 2\pi r_j dr_j = 2\pi r_j^2 d \log r_j$. Thus the power per logarithmic jet radius is

$$\frac{d\dot{E}}{d \log r_j} = p_j \frac{dA_\perp}{d \log r_j} \left(\frac{dz}{dt} \right) = p_j 2\pi r_j^2 v_h . \quad (11)$$

We define p_j as a function of r_j in the form (see Appendix A),

$$p_j(r_j) \approx p_h \begin{cases} 1 & (r_j < r_h) , \\ \left(\frac{r_j}{r_h} \right)^{-3} & (r_h < r_j < r_L) , \\ \left(\frac{r_L}{r_h} \right)^{-3} \left(\frac{r_j}{r_L} \right)^{-4} & (r_h < r_L < r_j) , \\ \left(\frac{r_j}{r_h} \right)^{-4} & (r_L < r_h < r_j) , \end{cases} \quad (12)$$

where

$$p_h \approx \rho_{\text{ext}} c^2 u_h^2 \quad (13)$$

is the pressure at the jet's head. The second and third cases in Eq. (12) are relevant only when the head is non-relativistic ($u_h \ll 1$), and therefore $r_h < r_L$ (see Eq. 2). The fourth case is relevant for a relativistic head. Figure 2 illustrates $p_j(r_j)$ in the different regimes.

A slightly different way of presenting $p_j(r_j)$ is by normalizing the pressure to $p_L = L_j/(\pi r_L^2 c)$, the jet's magnetic pressure at the light cylinder, which is constant for a given jet. This gives a sense of how the head's pressure depends on the ambient medium parameters:

$$p_j \approx p_L \begin{cases} \left(\frac{r_h}{r_L} \right)^{-4} \simeq a^{-2/3} & (r_j < r_h > r_L) , \\ \left(\frac{r_h}{r_L} \right)^{-3} \simeq a^{-3/5} & (r_j < r_h < r_L) , \\ \left(\frac{r_j}{r_L} \right)^{-3} & (r_h < r_j < r_L) , \\ \left(\frac{r_j}{r_L} \right)^{-4} & (\max\{r_L, r_h\} < r_j) . \end{cases} \quad (14)$$

Here, the first case is relevant for a relativistic head while the second and third cases are relevant for a non-relativistic head, as before.

Substituting Eq. (12) or (14) into Eq. (11) we obtain:

$$\frac{d\dot{E}}{d \log r_j} \propto \begin{cases} r_j^2 & (r_j < r_h), \\ r_j^{-1} & (r_h < r_j < r_L), \\ r_j^{-2} & (\max\{r_L, r_h\} < r_j). \end{cases} \quad (15)$$

Eq. (15) implies that the total pdV work performed by the jet on the ambient medium is dominated by the contribution from $r_j \leq r_h$. Therefore, the total rate of energy injection into the cocoon can be approximated as

$$\dot{E}_c \approx \pi p_h v_h r_h^2. \quad (16)$$

It is interesting to view the fraction of the jet luminosity that is transferred into the cocoon in this way. This is a measure of the efficiency of this process. Using Eqs. (2, 13) gives

$$\frac{\dot{E}_c}{L_j} \sim \frac{\pi \rho_{\text{ext}} c^3 r_L^2 u_h^4 \beta_h}{L_j} \sim \frac{u_h^4 \beta_h}{a} \sim \frac{1}{\Gamma_h^2}. \quad (17)$$

This implies that when the head of the jet is non-relativistic ($u_h \ll 1$) most of the source luminosity is channeled into the cocoon through the work performed by the head. However when the head becomes relativistic ($u_h \gg 1$) this fraction decreases by a factor of $1/\Gamma_h^2 \ll 1$. A similar ratio of \dot{E}_c/L_j was found in hydrodynamic jets as well (Bromberg et al. 2011a).

In order to calculate the cocoon's geometry, as parameterized by its cylindrical radius $r_c(z)$, we treat separately the region where the cocoon is relativistically hot ($p_c \gg \rho_{\text{ext}} c^2$), and the region where it is Newtonian ($p_c \ll \rho_{\text{ext}} c^2$). The former region exists only in jets with $u_h \gg 1$. It is characterized by a relativistic expansion of the cocoon and in the case of a collapsar jet it is limited to a narrow range near the head of the jet (see Fig. 1). The analysis in this region is done under the approximation that the cocoon's shape is at a steady state in the rest frame of the head. This assumption is exact in the case when the ambient medium is uniform. In this case the head propagates at a constant velocity (see Eq. 8), and the geometry of the shock in the relativistic part of the cocoon is constant in time. As we show below, this steady state approximation holds for most situations that are relevant for collapsar jets. In the Newtonian cocoon region the gas motion is non-relativistic. Here we approximate the expansion of the cocoon as cylindrical in the frame of the ambient medium. In both cocoon regions we assume that the pressure is uniform in the \hat{r} direction.

4.1 The relativistic cocoon regime

We turn now to examine the rate of production of internal energy at the bow shock that separates the relativistic cocoon from the ambient medium. Unlike the usual analysis of

relativistic shocks we perform the analysis in the frame of the star. We first calculate the flow of rest mass M through the shock per logarithmic interval of r_c . In a time dt the shock covers a volume $dV_{<r_c} = \pi r_c^2 v_h dt$, where $dV_{<r_c}$ is the volume at radius $< r_c$. The mass that flows through the shock during the time interval dt is $dM_{<r_c} = \rho_{\text{ext}} dV_{<r_c}$ thus:

$$\frac{d^2 M}{dt d \log r_c} \equiv \frac{d\dot{M}}{d \log r_c} = 2\pi r_c^2 \rho_{\text{ext}} v_h . \quad (18)$$

The ratio of energy density to rest mass energy density downstream of the shock is: $e/\rho c^2 = \bar{\Gamma}$, where we define \bar{u} as the proper velocity perpendicular to the shock in the downstream frame, and $\bar{\Gamma}$ as the Lorentz factor associate with this velocity (e.g. Beloborodov & Uhm, 2006). The boost to the lab frame gives an additional factor of $\bar{\Gamma}$. Therefore the internal energy per particle of the shocked material, in the lab frame, is $\tilde{e}_{\text{int}}/\tilde{\rho} c^2 \equiv e\bar{\Gamma}/\rho c^2 - 1 = (\bar{\Gamma}^2 - 1) = \bar{u}^2$. The generation rate of total internal energy, E_{int} , behind the shock, as measured in the lab frame, is therefore

$$\frac{d\dot{E}_{\text{int}}}{d \log r_c} = \left(\frac{d\dot{M}}{d \log r_c} \right) \frac{\tilde{e}_{\text{int}}}{\tilde{\rho}} \simeq 2\pi r_c^2 \rho_{\text{ext}} c^2 \bar{u}^2 v_h \propto r_c^2 \bar{u}^2 . \quad (19)$$

In the limit of a strong shock, \bar{u} can also be approximated as the normal component of the upstream proper velocity in the frame where the shock is stationary (in our case it is the rest frame of the head), i.e.:

$$\bar{u} \simeq u_h \cos \alpha_c'' = \frac{u_h}{\sqrt{1 + \Gamma_h^2 \tan^2 \alpha_c}} . \quad (20)$$

The relativistic cocoon regime corresponds to the regime where $\bar{u} > 1$. It can be seen from Eq. (20) that in this regime, the cocoon is conveniently separated into two zones (see fig. 3 for illustration of the different cocoon regions):

1. The head of the cocoon, defined by the condition $\alpha_c \lesssim 1/\Gamma_h$ (or $\alpha_c'' \lesssim 1$), is identified with $r_c < r_h$.
2. The transition region, defined by $1/\Gamma_h \lesssim \alpha_c \lesssim 1$ (or $1/\Gamma_h \lesssim \pi/2 - \alpha_c'' \lesssim 1$). Here $\bar{u} \approx \beta_h / \tan \alpha_c > 1$, hence the bow shock is still relativistic.

At the cocoon's head the plasma moves upwards at a velocity u_h (in the lab frame), and the pressure is roughly uniform, $p_c \approx \rho_{\text{ext}} c^2 \bar{u}^2 \approx \rho_{\text{ext}} c^2 u_h^2 \approx p_h$. We have shown in section 3 that most of the energy is injected into the cocoon in this region. This energy is transferred downwards along the cocoon (in the head frame) heating new portions of plasma entering via the wings of the bow shock.

In the transition region the plasma motion is quite involved. Close to the head it is still relativistic, however it approaches $\bar{u} = 1$ at the interface with the Newtonian cocoon region

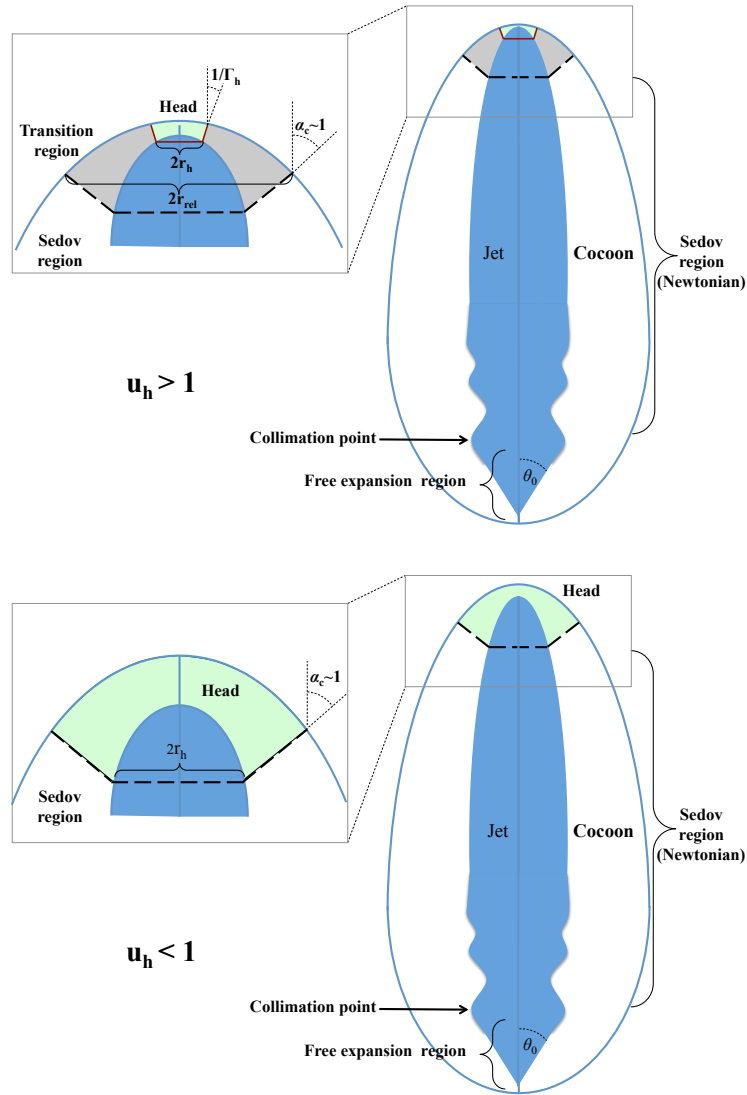


Figure 3: A schematic description of the different cocoon regions in a case of a relativistic head (top panel) and a non-relativistic head (bottom panel). In the relativistic case the cocoon is divided into three regions: a head (green), a transition region (gray) where the velocities are still relativistic, and a Newtonian region (white), which behaves like a cylindrical Sedov-Taylor blast wave. In the non-relativistic case the transition region disappears, leaving only the head and the Newtonian, Sedov-Taylor, region.

(see fig. 3). The geometry of the transition region can be obtained using the assumption that it is at a steady state in the head's frame. Consider a sub-region of $r < r_c$ in the transition region. The mass is entering this sub-region through the bow shock at a rate $\dot{M}_{\text{ext}} = \pi r_c^2 \rho_{\text{ext}} \beta_h c$. The energy is entering this sub-region through the interface with the head (see fig. 3) at a rate $\dot{E}_c \simeq L/\Gamma_h^2$ (Eqs. 16, 17). Since the flow is at a steady state, mass and energy are flowing out, at r_c , in the same rate. Now, since in the lab frame $\dot{E}_c \sim \dot{M}_{\text{ext}} c^2 \bar{u}^2$ (e.g. Eq. 19), it implies that $\bar{u}^2 \sim \dot{E}_c/\dot{M}_{\text{ext}} c^2 \sim L_j/(\pi \rho_{\text{ext}} c^3 r_c^2 \Gamma_h u_h)$. Using Eqs. (9, 10) we get that this velocity is equal to

$$\bar{u} \approx u_h r_h / r_c. \quad (21)$$

On the other hand, $\tan \alpha_c = d\bar{z}/dr_c$, where $\bar{z} \equiv z_h - z$ is the distance from the jet's head in the lab frame (see Fig. 1), implying that $\bar{u} \approx \beta_h / \tan \alpha = \beta_h dr_c / d\bar{z}$. Assuming a functional shape of $r_c = \bar{z}^\epsilon$ we obtain that

$$\bar{u} \approx \epsilon \beta_h r_c / \bar{z}. \quad (22)$$

Equating Eq. (22) with Eq. (21) provides the profile of r_c in the transition region,

$$r_c \approx \sqrt{2 r_h \Gamma_h \bar{z}}, \quad (23)$$

and gives $\epsilon = 1/2$.

The pressure in the cocoon, $p_c(\bar{z})$, which we assume to be nearly independent of r , can be estimated just behind the shock:

$$p_c \approx \rho_{\text{ext}} c^2 \bar{u}^2 = \rho_{\text{ext}} c^2 \left(\frac{\beta_h r_c}{2\bar{z}} \right)^2, \quad (24)$$

where we used Eq. (22) for \bar{u} . Substituting r_c from Eq. (23) we obtain:

$$p_c \approx p_h \frac{r_h}{2\Gamma_h \bar{z}} = p_h \beta_h \frac{r_L}{2\bar{z}}, \quad (25)$$

where we use the relation $p_h = \rho_{\text{ext}} c^2 u_h^2$. The jet radius is calculated using $r_j = r_h (p_h/p_c)^{1/4}$ (Eq. 3), resulting in:

$$r_j \approx r_h \left(\frac{2\bar{z}}{\beta_h r_L} \right)^{1/4}, \quad (26)$$

Note that $\bar{u} \propto r_c^{-1}$ as we show in Eq. (20) implies that $d\dot{E}_{\text{int}}/d\log r_c = \text{const}$, (Eq. 19). This means that most of the energy, which was injected by the jet at $r_c \lesssim r_h$ is given to newly shocked material each dynamical time. Such a behavior is expected in an adiabatic (i.e. constant energy) blast wave solution, like the Blandford-McKee or Sedov-Taylor solutions. In both cases $E \sim M\bar{u}^2$ and $M \propto r_c^2$. This type of solutions apply also to the regime where the shock becomes Newtonian, as we show in the next section.

We can now examine the assumption of a uniform ρ_{ext} in the relativistic cocoon regime. The transition point from a relativistic shock to a Newtonian shock occurs when $\bar{u} = 1$. From Eqs. (21, 22) we obtain that this occurs when

$$\bar{z} \equiv \bar{z}_{\text{rel}} \approx \frac{1}{2} r_{\text{L}} u_{\text{h}}^2 \beta_{\text{h}} \quad \text{and} \quad r_{\text{c}} \equiv r_{\text{rel}} \approx r_{\text{L}} u_{\text{h}}^2 \approx 2z_{\text{rel}}. \quad (27)$$

For any reasonable values of jet luminosity and stellar properties the Lorentz factor of the jet's head remains $u_{\text{h}} \lesssim 10$, until it breaks out of the stellar surface. Taking a reasonable estimation for the light cylinder radius, $r_{\text{L}} \simeq 10^7$ cm, results in a relativistic region of size $\bar{z}_{\text{rel}} \lesssim 10^9$ cm which is about two orders of magnitude smaller than the size of the jet before it breaks out of the star. In addition, the density of the stellar envelope changes on length scales much larger than 10^9 cm at this region (e.g. Mizulta & Alloy 2009). Deeper in the star the size of the relativistic region decreases roughly linearly with z_{h} for typical density profiles, and it remains smaller than $\rho_{\text{ext}}/|\nabla\rho_{\text{ext}}|$ throughout the entire star. Thus the approximation of a constant ambient medium density at the relativistic cocoon region is justified.

4.2 The Newtonian cocoon regime

When $\alpha_c \gtrsim 1$ ($\alpha_c'' \gtrsim \pi/2 - 1/\Gamma_{\text{h}})^2$, the shock becomes Newtonian ($\bar{u} < 1$). This region covers most of the jet while it is still inside the star. When the head of the jet is sub-relativistic it engulfs the entire jet (see Fig. 3). Here we cannot ignore the density gradient in the stellar envelope and thus the approximation of a steady state shock doesn't apply. Namely, while the relation $p_{\text{c}} \approx \rho_{\text{ext}} c^2 \bar{u}^2$ still holds, Eq. (20) can no longer be used to evaluate \bar{u} (the relative proper velocity between the upstream and the downstream). Instead we use the assumption that all motions in this region are in the $\hat{\mathbf{r}}$ direction, and that the expansion follows a cylindrical Sedov-Taylor solution, a low energy extension to the cylindrical Blandford-MaKee solution that was used in the relativistic cocoon region. In this type of expansion the cylindrical radius follows:

$$r_{\text{c}}^2(z) = 2\sqrt{\frac{\mathcal{E}(z)}{\pi\rho_{\text{ext}}(z)}}\Delta t, \quad (28)$$

where $\mathcal{E}(z)$ is the energy per unit length that was injected by the head when it passed through altitude z (i.e. when $z_{\text{h}} = z$):

$$\mathcal{E}(z) \equiv \frac{dE_{\text{c}}(z)}{dz} = \frac{\dot{E}_{\text{c}}(z)}{v_{\text{h}}(z)} \simeq \frac{L_{\text{j}}}{\Gamma_{\text{h}}(z)u_{\text{h}}(z)c}, \quad (29)$$

and we used Eqs. (16, 17) to express it in terms of the jet luminosity. Hereforth we use the terms $\Gamma_{\text{h}}(z)$, $u_{\text{h}}(z)$ and $v_{\text{h}}(z) = c\beta_{\text{h}}(z)$ to express the head's Lorentz factor, proper velocity

²The condition $\alpha_c \gtrsim 1$ is relevant also in the case when the head velocity is sub relativistic. In this case the region with $\alpha_c \lesssim 1$ is occupied by the head (see Fig. 3).

(i.e. the spatial part of the 4-velocity) and 3-velocity respectively, when the head passes altitude z (this terminology also applies below to $a(z)$, $z_{\text{rel}}(z)$ and $r_{\text{rel}}(z)$). The numerical coefficient $2/\sqrt{\pi} \simeq 1$, in Eq. (28) was chosen to obtain a smooth transition between the relativistic and the Newtonian cocoon regions.

To calculate $r_c(z)$ we need to evaluate Δt , the time that is available for the cocoon to expand since the energy is injected when the head crosses altitude z , until it reaches $z_h(t)$. We can use the substitution $dt \equiv dz_h/\beta_h(z)c$ and integrate over the propagation time of the head between the two limits. In order to obtain useful analytic expressions we use a power-law external density profile, $\rho_{\text{ext}} \propto z^{-\xi}$ with $\xi \geq 0$, and denote by z_1 the altitude where the jet's head becomes relativistic, namely $u_h(z_1) \equiv 1$, so that to a zero order

$$\beta_h(z) = \begin{cases} a(z)^{1/5} = (z/z_1)^{\xi/5} & (z < z_1), \\ 1 & (z > z_1). \end{cases} \quad (30)$$

Note that this also implies $u_h(z) \simeq \min[(z/z_1)^{\xi/5}, (z/z_1)^{\xi/6}]$.

We distinguish between three cases: a non-relativistic head ($z < z_h < z_1$), a relativistic head at z ($z_1 < z < z_h$), and a case where the head is non relativistic at altitude z but becomes relativistic before it reaches z_h ($z < z_1 < z_h$). This gives:

$$c\Delta t = \int_z^{z_h(t)} \frac{dz}{\beta_h(z)} = \begin{cases} \frac{5}{5-\xi} \left(\frac{z_h(t)}{\beta_h(z_h)} - \frac{z}{\beta_h(z)} \right) & (z < z_h < z_1), \\ \frac{5}{5-\xi} \left(z_1 - \frac{z}{\beta_h(z)} \right) + z_h(t) - z_1 & (z < z_1 < z_h), \\ z_h(t) - z & (z_1 < z < z_h), \end{cases} \quad (31)$$

Altogether the solution to Eq. (28) is

$$r_c^2(z, t) = 2r_L \begin{cases} \left(\frac{z}{z_1} \right)^{2\xi/5} \frac{5}{5-\xi} \left(\frac{z_h(t)}{\beta_h(z_h)} - \frac{z}{\beta_h(z)} \right) & (z < z_h < z_1), \\ \left(\frac{z}{z_1} \right)^{2\xi/5} \left[\frac{5}{5-\xi} \left(z_1 - \frac{z}{\beta_h(z)} \right) + z_h(t) - z_1 \right] & (z < z_1 < z_h), \\ \left(\frac{z}{z_1} \right)^{\xi/3} [z_h(t) - z] & (z_1 < z < z_h). \end{cases} \quad (32)$$

The cocoon pressure is evaluated as $p_c(z, t) \simeq \mathcal{E}(z)/\pi r_c^2(z, t)$, where we use the assumption that the pressure is roughly uniform in the $\hat{\mathbf{r}}$ direction

$$p_c(z, t) \simeq \frac{\rho_{\text{ext}}(z)c^2 u_h(z)^2}{2} r_L \begin{cases} \frac{5-\xi}{5} \left(\frac{z_h(t)}{\beta_h(z_h)} - \frac{z}{\beta_h(z)} \right)^{-1} & (z < z_h < z_1), \\ \left[\frac{5}{5-\xi} \left(z_1 - \frac{z}{\beta_h(z)} \right) + z_h(t) - z_1 \right]^{-1} & (z < z_1 < z_h), \\ (z_h(t) - z)^{-1} & (z_1 < z < z_h). \end{cases} \quad (33)$$

Note that $\rho_{\text{ext}}(z)c^2u_h(z)^2$ is just the pressure at the jet's head when it passes the altitude z . The jet's radius satisfies $r_j = r_L(p_L/p_c)^{1/3}$ when $r_j < r_L$ and $r_j = r_L(p_L/p_c)^{1/4}$ when $r_j > r_L$. Substituting p_c from Eq. (33) and using $p_L = L_j/(\pi r_L^2 c)$ we obtain

$$r_j(z, t) = r_L \begin{cases} \left(\frac{z}{z_1}\right)^{\xi/5} \left(\frac{2\kappa}{r_L}\right)^{1/3} \left(\frac{z_h(t)}{\beta_h(z_h)} - \frac{z}{\beta_h(z)}\right)^{1/3} & (z < z_h < z_1; r_j < r_L), \\ \left(\frac{z}{z_1}\right)^{3\xi/20} \left(\frac{2\kappa}{r_L}\right)^{1/4} \left(\frac{z_h(t)}{\beta_h(z_h)} - \frac{z}{\beta_h(z)}\right)^{1/4} & (z < z_h < z_1; r_j > r_L), \\ \left(\frac{z}{z_1}\right)^{3\xi/20} \left(\frac{2\kappa}{r_L}\right)^{1/4} \left(z_1 - \frac{z}{\beta(z)} + \frac{z_h(t) - z_1}{\kappa}\right)^{1/4} & (z < z_1 < z_h), \\ \left(\frac{z}{z_1}\right)^{\xi/6} \left(\frac{2\kappa}{r_L}\right)^{1/4} (z_h(t) - z)^{1/4} & (z_1 < z < z_h). \end{cases} \quad (34)$$

where $\kappa = 5/(5 - \xi)$ when $z < z_1$ and $\kappa = 1$ when $z > z_1$. Eqs. (32 – 34) describe the geometries of the cocoon and of the jet in the Newtonian region.

To illustrate the jet's and the cocoon's shape in our model we plot in fig. 4 the results of $r_j(z, z_h)$ and $r_c(z, z_h)$, calculated with four different density profiles. To demonstrate the temporal evolution of the jet in each profile, we perform the calculation at $z_h/z_1 = 0.3, 1, 3$. In all cases we use $r_L = 0.01z_1$. In fig. 5 we show a comparison of our model to a numerical simulation of a Poynting dominated collapsar jet (Bromberg & Tchekhovskoy, 2014). The figure shows snapshots of density (left panel), proper velocity (middle panel) and the pressure (right panel) taken 2 sec after the initiation of the jet. In each panel we plot in gray lines our analytic calculation of $r_j(z, t)$ (Eqs. 26, 34) and $r_c(z, t)$ (Eqs. 23, 32) at the same time of the snapshots. The radius of the simulated jet is best observed in the proper velocity panel, since u_j is expected to reach its peak value close to the interface with the cocoon. The analytically calculated r_j tracks the location of this peak remarkably well. There is also a very good match in p_c and r_c between the simulation and our model. The simulation and the analytic calculation were conducted using a star with $M = 15M_\odot$, $R = 10^{11}$ cm and a powerlaw density profile, $\rho_{\text{ext}} \propto z^{-2.5}$. The jet parameters are $L_j = 10^{50}$ erg/s and $r_L = 5 \times 10^7$ cm. The full details of the comparison are given in Bromberg & Tchekhovskoy (2014).

5 The collimation of the jet at the base

When the jet pushes its way through the stellar material, the cocoon pressure is generally large enough to confine the flow into a narrow channel such that the condition of strong connection is fulfilled. This can be checked by verifying that the condition (1) is fulfilled. Close to the injection point the jet's pressure is larger than the cocoon's pressure. Thus, the jet initially expands freely until it reaches a point where its internal pressure matches the pressure in the cocoon. From this point on the jet becomes collimated (see Fig. 1). The behavior of the jet above the collimation point depends on the causal connection across

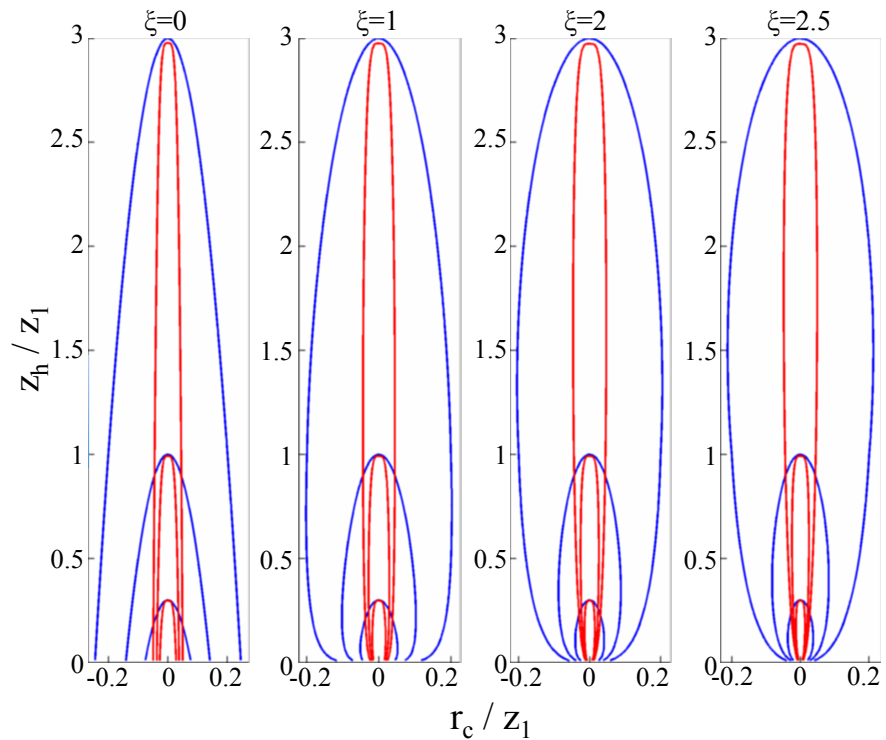


Figure 4: A schematic drawing of the jet (red) and the cocoon (blue) in four different density profiles: $\rho_{\text{ext}} \propto z^{-\xi}$, and in three altitudes: $z_h/z_1 = 0.3, 1, 3$. Length scales are normalized to z_1 , and we chose $r_L/z_1 = 0.01$.

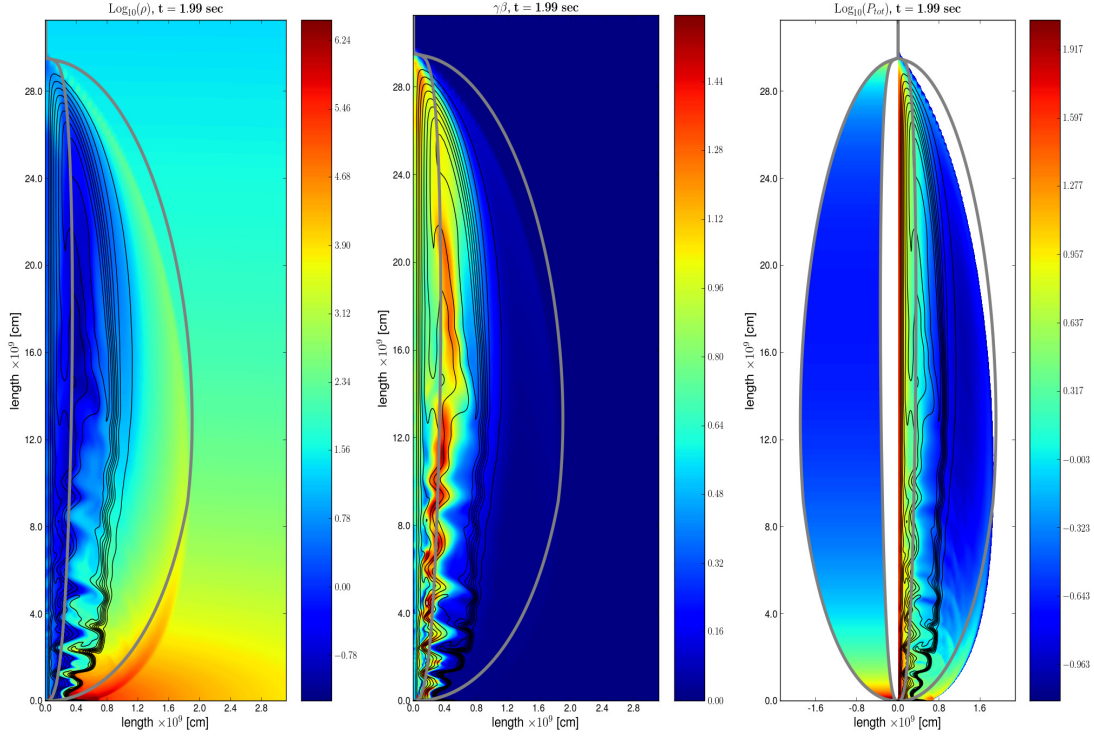


Figure 5: A comparison of the analytic model to a 2D simulation of a Poynting dominated collapsar jet from Bromberg & Tchekhovskoy (2014). We show snapshots taken 2 sec after the jet is initiated. Left panel depicts $\log_{10} \rho$ in units of g/cm^3 ; middle panel: $u = \Gamma\beta$; and right panel: $\log_{10}(p)$ in units of $10^{20} \text{ erg}/\text{cm}^3$. In the right, pressure, panel we show the simulated pressure on the right and the analytic calculation of $p_c(z, t)$ on the left. The thick gray lines mark the analytic values of $r_i(z, t)$ (inner line) and $r_c(z, t)$ (outer line) calculated at the same time as the snapshots. The heights of the analytic results are normalized by a factor of 1.3 to match the height of the simulated jet. For further details see Bromberg & Tchekhovskoy (2014)

the jet at the collimation point (see section 2). If causal contact between the outer part of the jet and the axis is still maintained at that point, the collimation is expected to occur without shocks or dissipation of energy. In this situation the jet energy remains dominated by Poynting flux all the way to the head.

We turn now to review the conditions near the foot of a collapsar's jet and determine the circumstances under which the cocoon's pressure is sufficient to collimate the jet while the jet still maintains causal connection with the axis. Suppose that the central engine produces a Poynting dominated jet with a (moderate) Lorentz factor $\Gamma_0 \approx 1$, a magnetization $\sigma_0 \gg 1$ and with an opening angle $\theta_j \geq \Gamma_0^{-1}$. Close to the central engine, the pressure of the jet exceeds the pressure in the cocoon, thus the flow expands freely. Such an unconfined flow expands radially, preserving the initial angle. It accelerates linearly up to the Lorentz factor $\Gamma_{cr} \sim (\sigma_0/\theta_j^2)^{1/3}$, after which it loses the causal contact and practically stops accelerating (Beskin, Kuznetsova & Rafikov, 1998; Tchekhovskoy, Narayan & McKinney, 2010). This occurs at the distance

$$z_{cr} \equiv r_L \Gamma_{cr} / \theta_j = r_L \sigma_0^{1/3} \theta_j^{-5/3}. \quad (35)$$

Above this point the jet material is no longer causally connected with the axis. Therefore the condition for the collimation to occur at $z \leq z_{cr}$ is

$$p_j(z_{cr}) \leq p_c(z_{cr}). \quad (36)$$

The magnetic pressure of the jet at z_{cr} is obtained by taking the condition (3) and substituting $r_j = z_{cr} \theta_j$:

$$p_j(z_{cr}) \simeq p_L \left(\frac{r_L}{\theta_j z_{cr}} \right)^4 = \frac{L_j}{\pi r_L^2 c} \sigma_0^{-4/3} \theta_j^{8/3}, \quad (37)$$

where $p_L = L_j / (\pi r_L^2 c)$ is the jet's pressure at the light cylinder. A lower limit on the cocoon's pressure at z_{cr} can be calculated by taking Eq. (33) in the limit where $u_h(z) > 1$ (assuming $z_{cr} < z_1 < z_h$):

$$p_c(z_{cr}) \simeq \frac{\rho_{ext}(z_{cr}) c^2 u_h(z_{cr})^2 r_L}{2} \left[z_h - \frac{5}{5 - \xi} \frac{z_{cr}}{\beta_h(z_{cr})} - \frac{\xi}{5 - \xi} z_1 \right]^{-1} \quad (38)$$

Comparison of $p_j(z_{cr})$ with $p_c(z_{cr})$ and requiring the condition (36) yields a lower limit on the value of the magnetization, σ_0 :

$$\sigma_0^{4/3} \geq \frac{2a(z_{cr})}{u_h^2(z_{cr}) r_L} \left[z_h - \frac{5}{5 - \xi} \frac{z_{cr}}{\beta_h(z_{cr})} - \frac{\xi}{5 - \xi} z_1 \right] \theta_j^{8/3} \quad (39)$$

Substitution of $z_h = R$, the stellar radius, ($R \gg [z_{cr}/\beta_h(z_{cr}), z_1]$) in the above expression gives the minimal value of σ_0 for which a jet, prior to its breakout, is collimated while it is

still causally connected. Approximating the stellar density as $\rho \propto z^{-\xi}$ we obtain that the minimal value of σ_0 is

$$\sigma_0^{4/3-\xi/5} \geq a_L^{3/5} \frac{R}{r_L} \theta_0^{8/3-\xi} = 5 \left[\frac{0.5}{3-\xi} L_{50} \left(\frac{15M_\odot}{M} \right) R_{11}^{(14/3-\xi)} r_{L,7}^{(\xi-11/3)} \right]^{3/5} \theta_j^{8/3-\xi}, \quad (40)$$

where $a_L \equiv a(z = r_L)$, M is the mass of the star and R is its radius. For a typical value of $\xi = 2.5$ we get that $\sigma_0 \gtrsim 10$. The values of σ_0 that are inferred in GRB jets, if they are dominated by Poynting flux, are typically above a few times 10^2 , at least an order of magnitude larger than this limit. With these values the jet is collimated smoothly prior to its breakout, without formation of internal shocks.

6 Stability of the jet

Our axisymmetric model implicitly assumes that the jet is not destroyed by global MHD instabilities. For a narrow jet, the most dangerous instability is the kink instability. This instability excites large-scale helical motions that can strongly distort or even disrupt the jet, thus triggering violent magnetic dissipation (Lyubarskij, 1992; Eichler, 1993; Spruit, Foglizzo & Stehle, 1997; Begelman, 1998; Lyubarskii, 1999; Giannios & Spruit, 2006). The instability can develop only in strongly causally connected flows, like a collimated jet. Therefore the Poynting dominated jet can survive the crossing of the star only if the crossing time is shorter than the growth time of the instability in the lab frame.

The kink instability is sensitive to the structure of the magnetic field in the flow. Flows with a purely toroidal field are mostly sensitive to disruption by this instability (Mignone et al., 2010; O’Neill, Beckwith & Begelman, 2012). Such a configuration could however be maintained in a strongly causally connected flow, only if the hoop stress is balanced by the plasma pressure and/or by the centrifugal force. This is possible only when $\sigma \leq 1$. Such a situation is relevant for pulsar wind nebulae, where the kink instability plays indeed a crucial role (Begelman, 1998; Porth, Komissarov & Keppens, 2014). In a strongly connected Poynting dominated flow, as in our case, in the comoving frame the toroidal field is comparable to the poloidal field (Lyubarsky, 2009). This results in a more stable flow.

In the simplest case of a, non-rotating, rigidly moving jet, the electric field vanishes in the comoving frame, and the hoop stress is balanced by the magnetic pressure. Thus the poloidal field decreases outwards. In this case, a characteristic time for the growth of a perturbation is about a few Alfvén radial crossing times in the comoving frame. For example, Appl, Lery & Baty (2000) found the growth rate $\kappa = 0.133v_A/r_j$ for a jet with $B_z(r) = B_0 r_j^2 / (r_j^2 + r^2)$, where v_A is the Alfvén velocity, which in our case could be taken to be equal to the speed of light. The full development of the instability takes generally a few characteristic growth times. One can estimate the total time necessary for the full development of the instability as $t'_{\text{kink}} \sim 10f/\kappa \approx 100fr_j/c$, where f is a numerical factor

having a value $f \sim 0.5 - 1$. This estimate agrees with the results of numerical simulations (Mizuno et al., 2009, 2012). The unstable perturbation propagates with the plasma of the jet therefore in the observer frame, the instability disruption time is estimated as

$$t_{\text{kink}} = \Gamma_j t'_{\text{kink}} \sim 100f \frac{r_j^2}{cr_L}, \quad (41)$$

where we used Eq. (2) to convert Γ_j . This time should be compared with the dynamical time that is available for the instability to grow in the jet. The relevant dynamical time, t_{dyn} , is the smaller between the propagation times of a fluid element to the jet's head and to the star's edge ($\approx R/c$).

When the head is Newtonian ($u_h \ll 1$) a fluid element crosses the jet at a time that is much shorter than the time it takes the jet to double its height. Therefore we can treat the jet as if it is stationary during the time it takes the fluid element to reach the head. Namely the fluid element tracks the time independent geometry of the jet, $r_j(z, z_h)$. To estimate the height of the widest point of the jet we take the derivative of $r_j(z, z_h)$ in Eq. (34) with respect to z , keeping z_h constant:

$$\left(\frac{\partial r_j}{\partial z} \right)_{z_h} = \frac{r_j}{z} \left[\frac{3\xi}{20} - \frac{5-\xi}{20} \left(\frac{z^{(5-\xi)/5}}{z_h^{(5-\xi)/5} - z^{(5-\xi)/5}} \right) \right]. \quad (42)$$

The jet's radius, $r_j(z, z_h)$, has an extremum at:

$$z_{\text{max}} \equiv z(\partial r_j / \partial z = 0) = 0.56 z_h \left(\frac{3\xi}{0.75(5+2\xi)} \right)^{\frac{5}{5-\xi}}. \quad (43)$$

A fluid element that is injected at the base of the jet expands as long as $z < z_{\text{max}}$. To estimate the growth of the kink instability during the expansion phase we compare t_{kink} (Eq. 41) with the time that passed since the injection, $t_{\text{dyn}} = z/c$, resulting in:

$$\frac{t_{\text{kink}}}{t_{\text{dyn}}} \Big|_{z < z_{\text{max}}} \simeq 200f \left(\frac{z}{z_1} \right)^{\frac{3\xi-10}{10}} \left(\frac{z_h}{z_1} \right)^{\frac{5-\xi}{10}} \left(\frac{r_L}{z_1} \right)^{1/2} \left(\frac{2.5}{5-\xi} \right)^{1/2} \left[1 - \left(\frac{z}{z_h} \right)^{\frac{5-\xi}{5}} \right]^{1/2}. \quad (44)$$

For $z < z_{\text{max}}$ this ratio scales like $z^{-0.25+0.3(\xi-2.5)}$, therefore it is minimal, or least stable, at $z = z_{\text{max}}$:

$$\frac{t_{\text{kink}}}{t_{\text{dyn}}} \Big|_{z=z_{\text{max}}} \simeq 10f \left(\frac{z_1}{2.5 \times 10^9} \right)^{-1/2} r_{L,7}^{1/2} \left(\frac{z_h}{z_1} \right)^{\frac{\xi-2.5}{5}} \left(\frac{2.5}{5-\xi} \right)^{1/2} \left(\frac{3\xi}{0.75(5+2\xi)} \right)^{\frac{3\xi-10}{2(5-\xi)}}. \quad (45)$$

Implying that the instability doesn't have enough time to grow in the expanding part of the jet.

The fluid element stops expanding at $z = z_{\max}$ and from there on its radius decreases until it reaches the head. The dynamical time available for the instability to evolve now is $t_{\text{dyn}} = \bar{z}/c$, resulting in the ratio

$$\left. \frac{t_{\text{kink}}}{t_{\text{dyn}}} \right|_{z > z_{\max}} \gtrsim 200 f \left(\frac{z_{\max}}{z_1} \right)^{3\xi/10} \left(\frac{r_L}{\bar{z}} \right)^{1/2} \left(\frac{2.5}{5-\xi} \right)^{1/2}, \quad (46)$$

where we approximated in r_j , $\beta_h(z) \simeq \beta_h(z_{\max})$, and $z_h/\beta_h - z/\beta_h(z) \gtrsim \bar{z}$, which gives a lower limit to t_{kink} . Using our fiducial parameters we get that $t_{\text{kink}}/t_{\text{dyn}} \sim 10f(z_{\max}/\bar{z})^{1/2}$, which implies that the time available for the instability to grow decreases faster than the growth time of the instability. Implying that the kink instability cannot grow in the region where the jet's head is non-relativistic.

When the head is relativistic ($u_h \gg 1$), the flow velocity is very close to the velocity of the head. Here we cannot neglect the motion of the head during the propagation of the fluid element. Namely, as a fluid element propagates from altitude z to $z + \delta z$ the jet's head has moved from z_h to $z_h + \beta_h \delta z$ which implies that the geometry of the jet is changing during the motion of the fluid element. Thus in this limit we need to use the total derivative with respect to z :

$$\frac{dr_j(z, z_h)}{dz} = \frac{r_j}{z} \left[\frac{\xi}{6} - \frac{1 - \beta_h(z_h) z}{4 \bar{z}} \right], \quad (47)$$

where $r_j(z, z_h)$ is taken from Eq. (34) and we approximated $dr_h/dz \simeq \beta_h(z)$. The height of the maximal radius of a fluid element is obtained by taking $dr_j/dz = 0$. Giving

$$\bar{z}_{\max} \equiv z_h - z(dr_j/dz = 0) \simeq 0.6 z_h (1 - \beta_h) \frac{2.5}{\xi} \quad (48)$$

Note that unlike in the case of a non-relativistic head, \bar{z}_{\max} here is located above the widest point of the jet, which is a direct consequence of the fact that the jet's pattern expands at a comparable rate to the propagation rate of the fluid element.

In the region where the fluid element expands, $z < z_{\max}$, the dynamical time is $t_{\text{dyn}} = z/c$, similar to the non relativistic head. In this case the ratio of $t_{\text{kink}}/t_{\text{dyn}}$ gives

$$\left. \frac{t_{\text{kink}}}{t_{\text{dyn}}} \right|_{z < z_{\max}} \gtrsim 140 f \frac{r_L}{z_1} \left(\frac{z}{z_1} \right)^{\frac{\xi-3}{3}} \left(\frac{\bar{z}}{r_L} \right)^{1/2}. \quad (49)$$

From Eq. (47) we can see that as long as $z \ll \bar{z}/(1 - \beta_h) \simeq 2\Gamma_h^2 \bar{z}$, the fluid element expands like $r_j(t) \sim z^{\xi/6}$ when it moves from z to $z + \delta z$. Therefore during the expansion phase $t_{\text{kink}}/t_{\text{dyn}} \propto z^{-0.17(3-\xi)/0.5}$, implying that instability growth is inhibited by the increasing in the cylindrical radius. The jet is least stable at $z = z_{\max}$, where we get

$$\left. \frac{t_{\text{kink}}}{t_{\text{dyn}}} \right|_{\bar{z} = \bar{z}_{\max}} \gtrsim 4f r_{L,7}^{1/2} z_{h,11}^{(\xi-3)/6} \left(\frac{z_1}{2.5 \times 10^9} \right)^{-\xi/6} \left(\frac{\xi}{2.5} \right)^{1/2}, \quad (50)$$

which implies again that the jet is most likely stable below z_{\max} .

Above z_{\max} the radius of the fluid element decreases with z . Since the head is propagating relativistically, the time that is left for the instability to grow is $t_{\text{dyn}}(\bar{z}_{\max}) = \bar{z}_{\max}/(1 - \beta_h) \simeq 0.6z_h \frac{2.5}{\xi}$. Thus the time to reach the head is comparable to the time it takes to reach z_{\max} . We can therefore neglect the change in β_h during this remaining time, and write a general expression for $t_{\text{dyn}}(\bar{z}) = \bar{z}/(1 - \beta_h)$. Comparing this time with t_{kink} we get the ratio

$$\frac{t_{\text{kink}}}{t_{\text{dyn}}} \simeq 70f \left(\frac{r_L}{\bar{z}}\right)^{1/2} \simeq 6f r_{L,7}^{1/2} z_{h,11}^{(\xi-3)/6} \left(\frac{z_1}{2.5 \times 10^9}\right)^{-\xi/6} \left(\frac{\xi}{2.5}\right)^{1/2} \left(\frac{\bar{z}_{\max}}{\bar{z}}\right)^{1/2}, \quad (51)$$

which scales as $\bar{z}^{-1/2}$, like in the case of a non-relativistic head. We therefore conclude that unless f is very small, the jet will not be disrupted by kink instability as it propagates in the star. Even for values of $f \sim 0.1$, the jet will only be marginally unstable and is likely to survive the crossing of the star.

This analysis was performed under the assumption that the jet is not rotating and moves upward rigidly. In this case the poloidal field scales roughly like r^{-1} . In a more realistic scenario of a rotating, differentially moving jet, the electric field plays a role in the transverse force balance. Then the outward gradient of the poloidal magnetic field could be smaller than in the rigidly moving jet or even vanish altogether. Istomin & Pariev (1996) have shown that Poynting dominated jets with homogeneous poloidal field are stable. Lyubarskii (1999) considered the general case and found that the instability growth rate decreases at shallower profiles of the poloidal magnetic field and it goes to zero for a homogeneous field. Simulations of cylindrical jets with shallow transverse distribution of the poloidal field (Mizuno et al., 2012) indeed revealed slower perturbation growth in accord with linear stability analysis. More importantly, they clearly demonstrate a nonlinear saturation of the instability in this case so that the initial cylindrical structure is not disrupted. An important point is that simulations of jet launching by a spinning accreting black hole reveal that in these Poynting-dominated jets, the poloidal field is very close to uniform (Tchekhovskoy, McKinney & Narayan, 2008b). It suggests that such Poynting dominated jets could not be destroyed by the kink instability. This agrees with 3D simulations by McKinney & Blandford (2009) who did not observe the kink instability in Poynting dominated jets emanated from an accreting black hole.

These findings add credibility to our conclusion that the jet is stable. Nevertheless, we stress that our stability analysis is based on the results that are available in the literature, which use a somewhat different setup. In particular in our model the jet is bounded by a tangential discontinuity that separates it from the cocoon. The discontinuity as well as the cocoon don't exist in the cited works. This may affect both the growth rate and the non linear behavior of the kink instability, as well as potentially lead to additional instabilities. All these effects can be fully tested with numerical 3D simulations.

7 Explicit time dependence and the jet breakout time

The properties of the jet and the cocoon in our model depend on two parameters, t and z . So far it was convenient to include the time dependence implicitly thorough the (time dependent) location of the jet's head, $z_h(t)$. In this case we could also use the coordinate $\bar{z} \equiv z_h(t) - z$ instead of z in some situations. The explicit time dependence can be obtained by calculating $t(z_h)$, the time in which the jet's head reaches an altitude z_h :

$$t(z_h) = \int_0^{z_h} \frac{dz}{\beta_h(z)c} \simeq \int_0^{z_1} \left(\frac{z_1}{z}\right)^{\xi/5} \frac{dz}{c} + \int_{z_1}^{z_h} \left(1 + \frac{1}{2} \left(\frac{z_1}{z}\right)^{\xi/3}\right) \frac{dz}{c}. \quad (52)$$

Here we care about small differences from the speed of light thus we approximate

$$\frac{1}{\beta_h(z)} \simeq \begin{cases} a(z)^{-1/5} = (z_1/z)^{\xi/5} & (z < z_1) \\ [1 - a(z)^{-1/3}]^{-1/2} \simeq 1 + 1/2(z_1/z)^{\xi/3} & (z_1 < z) . \end{cases} \quad (53)$$

This gives the expression:

$$\frac{ct(z_h)}{z_h} \simeq \begin{cases} \frac{5}{5-\xi} \left(\frac{z_1}{z_h}\right)^{\xi/5} & (z_h < z_1) \\ 1 + \frac{3}{2(3-\xi)} \left(\frac{z_1}{z_h}\right)^{\xi/3} + \frac{z_1}{z_h} \left[\frac{\xi}{5-\xi} - \frac{3}{2(3-\xi)}\right] & (z_1 < z_h) . \end{cases} \quad (54)$$

In the case where $z_h \gg z_1$ and $\xi < 3$ the third term in Eq. (54,b) is negligible, while for $\xi > 3$ the second term can be neglected, allowing for an explicit solution of $z_h(t)$. Solving for z_h , and noting that when $z_h > z_1$, $\Gamma_h^2(z_h) \simeq \left(\frac{z_h}{z_1}\right)^{\xi/3}$ we get

$$z_h(t) \simeq \begin{cases} z_1 \left(\frac{5-\xi}{5} \frac{ct}{z_1}\right)^{5/(5-\xi)} & (z_h < z_1) \\ \left[ct - z_1 \left(\frac{\xi}{5-\xi} - \frac{3}{2(3-\xi)}\right)\right] \left[1 + \frac{3}{2(3-\xi)\Gamma_h^2(z_h)}\right]^{-1} & (z_h > z_1) , \end{cases} \quad (55)$$

This result can be substituted in Eqs. (23 – 34) in order to obtain the explicit time dependence of all the model parameters.

A typical collapsar jet becomes relativistic at

$$z_1 \simeq a(R)^{-1/\xi} R = 2.5 \times 10^9 \text{cm} \left[\left(\frac{3-\xi}{0.5}\right) L_{50}^{-1} \left(\frac{M}{15M_\odot}\right) r_{L,7}^2 \right]^{1/\xi} R_{11}^{1-3/\xi}, \quad (56)$$

Since $z_1 \ll R$ the jet becomes relativistic deep in the star and therefore we can approximate the time it breaks out of the stellar surface as

$$t_R \equiv t_h(z_h = R) \simeq \frac{R}{c} \left(1 + \frac{3}{2(3-\xi)a^{1/3}(R)}\right) = 3.3R_{11} \left(1 + 0.14 \left(\frac{0.5}{3-\xi}\right) a_4^{-1/3}(R)\right) \text{ s} . \quad (57)$$

where

$$a_4(R) \equiv \frac{a(R)}{10^4} = \left(\frac{0.5}{3 - \xi} \right) L_{50} r_{L,7}^{-2} \left(\frac{M}{15 M_\odot} \right)^{-1} R_{11}^3. \quad (58)$$

Thus the jet reaches the stellar surface after $t_R \simeq 4$ s, which is only slightly longer than the light crossing time of the star.

Last, we calculate the minimal activity time of the engine that is required to push the jet out of the star. When the jet propagates in the star, part of its energy is deposited into the cocoon. It follows that the engine needs to invest some minimal amount of energy to push the jet out of the star, corresponding with a minimal activity time. The rest of the energy is available to produce the observed GRB emission. When the jet engine stops the information that this has happened propagates upward at the fast magnetosonic speed, in the fluid rest frame, which is very close to the speed of light. During that time the head of the jet continues to move forward as if nothing has happened. If this information reaches the head before the head breaks through the stellar surface, the jet will slow down and fail to breakout. We define the threshold activity time for a successful jet breakout, $t_{\text{th}} = t_R - R/c$, as the difference between the breakout time, t_R , and the light crossing time, R/c , of the star. If the engine stops at $t < t_{\text{th}}$ the jet will fail to exit the star. In cases when the head of the jet is non-relativistic during the entire crossing, $t_R \gg R/c$; then $t_{\text{th}} \simeq t_R$. When the jet's head is relativistic the threshold time can be easily obtained by noting that $ct_{\text{th}}/R = (ct_R/R) - 1$ where ct_R/R is given by Eq. (57):

$$t_{\text{th}} \simeq \frac{2}{2(3 - \xi)} \frac{R}{c} a(R)^{-1/3} \simeq 0.5 \left[\left(\frac{0.5}{3 - \xi} \right)^2 L_{50}^{-1} \left(\frac{M}{15 M_\odot} \right) r_{L,7}^2 \right]^{1/3} \text{ s}. \quad (59)$$

As the jet becomes relativistic deep in the star this time is much shorter than t_R , the time it takes for the jet's head to reach the stellar surface. Note that t_{th} is the last time where any information that leaves the engine can reach the head before the jet breaks out of the star. Therefore we can estimate the maximal amount of energy that the jet can put into the stellar envelope as:

$$E_{c,\text{max}} = 2L_j t_{\text{th}} \simeq 10^{50} \text{ erg} \times \left[\left(\frac{0.5}{3 - \xi} \right)^2 L_{50}^{-1} \left(\frac{M}{15 M_\odot} \right) r_{L,7}^2 \right]^{1/3}, \quad (60)$$

where the factor of 2 is used to account for the two sides of the jet. This energy is well below the energy required to unbind the star, which is of the order of $\sim 1.5 \times 10^{51}$ ergs for our fiducial set of parameters. Implying that magnetic GRB jets by themselves cannot unbind their progenitor stars.

8 Conclusions

We have developed an analytic model for the propagation of a relativistic Poynting flux dominated jet in a dense medium and applied it to collapsar jets. Namely, to relativistic

jets produced within a collapsing star that propagate in their massive star progenitor. Note that we consider as collapsars all cases of GRB models that involves jets that propagate through their massive stellar progenitor, regardless of the nature of the central engine that powers them.

As the jet propagates it pushes the material in front of it, leading to the formation of a bow shock ahead of the jet. Matter that passes through this shock is heated and forms a cocoon, that applies pressure on the jet and collimates it. At the same time the cocoon propagates sideways into the stellar envelope. Inside the star the cocoon pressure is large enough to collimate the jet close to the launching point so that the jet's outer boundary maintains a strong lateral causal contact with its center. In this case the jet is collimated smoothly without dissipation, and therefore almost all of the magnetic flux reaches the head.

We have shown that both the size, r_h , and the proper velocity, u_h of the jet's head depend only on the ratio $(L_j/r_L^2)(1/\rho_{ext})$. The first factor depends on the total luminosity of the jet and the size of its central engine while the latter depends only on the external density profile. These quantities do not depend on the details of the jet structure behind its head. Since the energy is injected into the cocoon only at the jet's head, this enables us to analytically estimate the energy injection rate into the cocoon without the need to know the exact structure of the jet. Using this energy injection rate we calculate the cocoon's structure. Finally, once the cocoon pressure profile is known we determine the jet's structure. We show that the resulting jet structure is indeed consistent with the properties of the jet's head. In spite of the various approximations used, the analytic model is in a good agreement with the results (see Figure 5) of recent simulations (Bromberg & Tchekhovskoy, 2014).

The propagation of the Poynting flux dominated jet described here should be contrasted with the propagation of a similar hydrodynamic jet. The basic difference arises due to the fact that while strong shocks can form in a hydrodynamic flow they cannot arise in a Poynting flux dominated outflow (Kennel & Coroniti, 1984). Therefore in a hydrodynamic jet the head of the jet involves both a forward shock that propagates into the surrounding stellar material and a reverse shock that propagates into the jet's material and slows it down significantly. At the same time the pressure exerted by the cocoon on the jet leads to a collimation shock that takes place deep near the base of the jet (Komissarov & Falle, 1997; Bromberg & Levinson, 2007; Bromberg et al., 2011). This shock heats initially cold matter and slows it down. The interplay between these two shocks, the one at the head of the jet and the collimation shock at the base determines the hydrodynamic jet structure. Unlike the Poynting flux dominated jet the hydrodynamic jet is slow and for most relevant parameters its head propagates with sub-relativistic velocities. This means that the jet crossing time is longer and the energy deposited by the shock and given to the stellar envelope is larger by an order of magnitude than the corresponding quantities for the corresponding Poynting flux dominated outflow.

The most questionable assumption is that the magnetic jet remains axi-symmetric and

stable. Our estimates have shown that the kink instability, which is the fastest growing instability, is unlikely to disrupt the jet while it propagates in the star. It could, however, somewhat change the details of our results, for example it may increase somewhat the size the head and therefore decreases its velocity and subsequently increases the jet escape time. However our analysis is based on linear estimates of the growth rate of the instability and even those are somewhat approximate. Clearly only full three dimensional simulations could clarify the issue of stability.

Levinson & Begelman (2013) have analyzed recently a similar system reaching a very different conclusions. They have argued that such a magnetic dominated jet becomes unstable while propagating within the star. Due to this instability the jet dissipates its magnetic energy on a time scale that is much shorter than the jet propagation time. The jet continues propagating as a hydrodynamic jet within the star. The main difference between their analysis and ours is that Levinson & Begelman (2013) assume that the inner part of the cocoon is dominated by the pressure of toroidal magnetic fields, exerting a much larger pressure on the jet boundary. In addition they assume that the cocoon pressure is uniform in the z direction. These two assumptions result in a cylindrical jet having a width that is comparable to r_h . Such a narrow jet is unstable to kink instability. Overall we expect that the assumption of a toroidal magnetic pressure dominated region in the cocoon is not entirely justified. In particular numerical simulations (Bromberg & Tchekhovskoy, 2014) do not show such a structure.

When applying these results to collapsars we recall that the typical size of the head is a few light cylinder radii r_L and the propagation proper velocity is mildly relativistic ($u_h \sim r_h/r_L \sim$ a few) during most of the propagation inside the star. Thus, the jet crosses the star in a time that is close to its light crossing time, R/c . The fast head velocity implies that once the jet is launched it will most likely exit the star. The fast crossing time also implies that the energy injected into the star is minimal. Astrophysical implications of these finds will be discussed elsewhere (Bromberg et al., 2014).

Acknowledgements

We thank A. Tchekhoskoy, M. Kuntz, A Spitkovsky, J. Stone and A. Levinson for helpful discussions and the ISSI (Bern) for hospitality while the final version of this paper was written. This research was supported by the ERC advanced research grant “GRBs” by the I-CORE (grant No 1829/12), by HUI-USP grant and by the Max-Planck/Princeton Center for Plasma Physics.

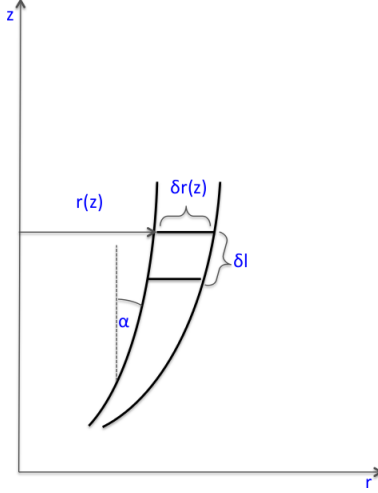


Figure 6: A schematic drawing of the jet element

A Basic derivation of the dependence of the jet properties on the inlet velocity of the flow

Let us consider the flow between two flux surfaces corresponding to $r(z)$ and $r(z) + \delta r(z)$ (see figure 6). The stream lines are along the poloidal field lines, in a direction \hat{e}_p that makes an angle α with the z -axis (see Fig. 6) so that

$$\cos \alpha = \left[1 + \left(\frac{dr}{dz} \right)^2 \right]^{-1/2}, \quad \sin \alpha = \left[1 + \left(\frac{dz}{dr} \right)^2 \right]^{-1/2}. \quad (61)$$

Let us now consider a fluid element of height δl along the poloidal direction. Flux freezing implies that the magnetic flux through a surface normal to the relevant magnetic field component is constant, implying that $\mathbf{B}_\phi \cdot (\delta \mathbf{r} \times \delta \mathbf{l}) = B_\phi \delta r \delta l \cos \alpha = \text{const}$; $\mathbf{B}_p \cdot (r \delta r) \hat{\mathbf{z}} = B_p r \delta r \cos \alpha = \text{const}$, and therefore $B_\phi / B_p \propto r / \delta l$, where B_ϕ and B_p are the azimuthal and poloidal magnetic field components, respectively. The mass of the fluid element scales as $\rho \Gamma \delta l r \delta r \cos \alpha$, while the rest mass flux (which is also conserved between two stream surfaces in steady state) scales as $\rho u r \delta r \cos \alpha$ (where $u = \Gamma \beta$ is the proper velocity). By taking the ratio of these two conserved quantities one obtains $\delta l \propto \beta$, which implies that $B_\phi / B_p \propto r / \beta$.

Now, since the jet is in lateral causal contact and thus in lateral equilibrium, the two components of the field are comparable in the comoving frame, $B'_\phi \sim B'_p$. Lorentz transformation of the fields to the lab frame (in which the central source and external medium are at rest), implies $B_\phi / \Gamma = B'_\phi \sim B'_p = B_p$, so that $\Gamma \sim B_\phi / B_p \propto r / \beta$ and $r \propto u = \Gamma \beta$. Near the light cylinder, at $r \sim r_\perp$, the two field components are comparable

in the lab frame and $u(r_L) \sim 1$, which implies that $u \sim r/r_L$. In the limit where $\cos \alpha \simeq 1$ we get that the magnetic pressure $p_B \sim (B'_\phi)^2 \sim (B_\phi/\Gamma)^2 \sim (\delta r u)^{-2} \sim r^{-4}$.

When the head of the jet is Newtonian ($u_h < 1$), the velocity of the jet material is non-relativistic in the part of the jet that holds $r_j/r_L \simeq u_j < 1$. In this region the approximation of a steady state in the lab frame breaks down. However, since most of the work done by the jet on the cocoon is performed at its head where, $r_j \leq r_h \simeq r_L u_h$, then in the region $r_h < r_j \leq r_L$ the energy flux in the lab frame is still constant and equal to L_j to a good approximation. Therefore, one can use Eq. (6) which shows that $L_j \propto r_j^2 \Gamma_j u_j p_j \propto p_j r_j^4 / \beta_j$. Implying that $p_j \propto \beta_j r_j^{-4}$. In the relativistic section of the jet ($r_j > r_L$), where $\beta_j \approx 1$, this recovers the above result of $p_j \propto r_j^{-4}$ (or $p_b \propto r^{-4}$, which shows that there the steady state approximation in the lab frame works well). In the Newtonian part of the jet, however ($r_j < r_L$), we get that $\beta_j \approx u_j \propto r_j$, therefore the scaling of the pressure with the jet radius changes to $p_j \propto r_j^{-3}$ (or $p_b \propto r^{-3}$).

References

- Appl S., Lery T., Baty H., 2000, *A&A*, 355, 818
- Begelman M. C., 1998, *ApJ*, 493, 291
- Beloborodov A. M., Uhm Z. L., 2006, *ApJ*, 651, L1
- Beskin V. S., Kuznetsova I. V., Rafikov R. R., 1998, *MNRAS*, 299, 341
- Bromberg O., Granot J., Piran T., Lyubarsky Y., 2014, in prep
- Bromberg O., Levinson A., 2007, *ApJ*, 671, 678
- Bromberg O., Nakar E., Piran T., Sari R., 2011, *ApJ*, 740, 100
- Bromberg O., Nakar E., Piran T., Sari R., 2012, *ApJ*, 749, 110
- Bromberg O., Tchekhovskoy A., 2014, in prep
- Eichler D., 1993, *ApJ*, 419, 111
- Giannios D., Spruit H. C., 2006, *A&A*, 450, 887
- Granot J., Cohen-Tanugi J., do Couto e Silva E., 2008, *ApJ*, 677, 92
- Granot J., Komissarov S. S., Spitkovsky A., 2011, *MNRAS*, 411, 1323
- Istomin Y. N., Pariev V. I., 1996, *MNRAS*, 281, 1
- Kawanaka N., Piran T., Krolik J. H., 2013, *ApJ*, 766, 31

Kennel C. F., Coroniti F. V., 1984, *ApJ*, 283, 710

Kohler S., Begelman M. C., 2012, *MNRAS*, 426, 595

Komissarov S. S., Barkov M. V., Vlahakis N., Königl A., 2007, *MNRAS*, 380, 51

Komissarov S. S., Falle S. A. E. G., 1997, *MNRAS*, 288, 833

Komissarov S. S., Vlahakis N., Königl A., Barkov M. V., 2009, *MNRAS*, 394, 1182

Lazzati D., Begelman M. C., 2005, *ApJ*, 629, 903

Levinson A., Begelman M. C., 2013, *ApJ*, 764, 148

Lithwick Y., Sari R., 2001, *ApJ*, 555, 540

Lyubarskii Y. E., 1999, *MNRAS*, 308, 1006

Lyubarskij Y. E., 1992, *Soviet Astronomy Letters*, 18, 356

Lyubarsky Y., 2009, *ApJ*, 698, 1570

Lyubarsky Y., 2010, *ApJ*, 725, L234

Lyubarsky Y., 2011, *Phys. Rev. E*, 83, 016302

MacFadyen A. I., Woosley S. E., 1999, *ApJ*, 524, 262

MacFadyen A. I., Woosley S. E., Heger A., 2001, *ApJ*, 550, 410

Matzner C. D., 2003, *MNRAS*, 345, 575

McKinney J. C., Blandford R. D., 2009, *MNRAS*, 394, L126

Michel F. C., 1969, *ApJ*, 158, 727

Mignone A., Rossi P., Bodo G., Ferrari A., Massaglia S., 2010, *MNRAS*, 402, 7

Mizuno Y., Lyubarsky Y., Nishikawa K.-I., Hardee P. E., 2009, *ApJ*, 700, 684

Mizuno Y., Lyubarsky Y., Nishikawa K.-I., Hardee P. E., 2012, *ApJ*, 757, 16

Mizuta A., Aloy M. A., 2009, *ApJ*, 699, 1261

Mizuta A., Ioka K., 2013, *ApJ*, 777, 162

Morsony B. J., Lazzati D., Begelman M. C., 2007, *ApJ*, 665, 569

O'Neill S. M., Beckwith K., Begelman M. C., 2012, *MNRAS*, 422, 1436

- Piran T., 1995, ArXiv Astrophysics e-prints
- Porth O., Komissarov S. S., Keppens R., 2014, MNRAS, 438, 278
- Spruit H. C., Foglizzo T., Stehle R., 1997, MNRAS, 288, 333
- Tchekhovskoy A., McKinney J. C., Narayan R., 2008a, in American Institute of Physics Conference Series, Vol. 1054, American Institute of Physics Conference Series, Axelsson M., ed., pp. 71–77
- Tchekhovskoy A., McKinney J. C., Narayan R., 2008b, MNRAS, 388, 551
- Tchekhovskoy A., McKinney J. C., Narayan R., 2009, ApJ, 699, 1789
- Tchekhovskoy A., Narayan R., McKinney J. C., 2010, New Astron., 15, 749
- Woosley S. E., 1993, ApJ, 405, 273
- Zakamska N. L., Begelman M. C., Blandford R. D., 2008, ApJ, 679, 990
- Zhang W., Woosley S. E., MacFadyen A. I., 2003, ApJ, 586, 356